JACS
JOURNAL OF THE AMERICAN CHEMICAL SOCIETY

Communication

pubs.acs.org/JACS

Efficiency Enhancement of Perovskite Solar Cells through Fast Electron Extraction: The Role of Graphene Quantum Dots

Zonglong Zhu,[†,‡] Jiani Ma,[⊥] Zilong Wang,[‡] Cheng Mu,[‡] Zetan Fan,[§] Lili Du,[⊥] Yang Bai,[‡] Louzhen Fan,*[,§] He Yan,[‡] David Lee Phillips,[⊥] and Shihe Yang*[,†,‡]

[†]Nano Science and Technology Program and [‡]Department of Chemistry, The Hong Kong University of Science and Technology, Clear Water Bay, Kowloon, Hong Kong

[⊥]Department of Chemistry, The University of Hong Kong, Pokfulam Road, Hong Kong S.A.R., P. R. China

[§]Department of Chemistry, Beijing Normal University, Beijing 100875, China

Supporting Information

ABSTRACT: We report on a significant power conversion efficiency improvement of perovskite solar cells from 8.81% to 10.15% due to insertion of an ultrathin graphene quantum dots (GQDs) layer between perovskite and TiO_2. A strong quenching of perovskite photoluminescence was observed at ~760 nm upon the addition of the GQDs, which is pronouncedly correlated with the increase of the IPCE and the APCE of the respective cells. From the transient absorption measurements, the improved cell efficiency can be attributed to the much faster electron extraction with the presence of GQDs (90−106 ps) than without their presence (260−307 ps). This work highlights that GQDs can act as a superfast electron tunnel for optoelectronic devices.

High-efficiency photovoltaics that uses solar radiation is attractive in meeting societal needs for energy, as it is clean and renewable.[1] Perovskite solar cells based on the $CH_3NH_3PbI_3$ sensitizer family have attracted great attention in terms of both mesoscopic[2,3] and planar heterojunctions,[4] with their power conversion efficiencies (PCEs) reaching >15%.[5,6] One prominent feature of the perovskites is that the electron/hole diffusion length has reached 100 nm in the triiodide absorber ($CH_3NH_3PbI_3$)[7] and >1 μm in the mixed halide absorber ($CH_3NH_3PbI_{3-x}Cl_x$),[8] all much longer than in current low-temperature solution-processed photovoltaic materials (typically ~10 nm).[9] This, together with a broad spectral absorption, a high open circuit voltage, etc., has aroused enthusiastic optimism among researchers over the potential of perovskite solar cells to achieve PCEs of >20%.[10,11] However, the injection times of electrons and holes in perovskite solar cells have been measured to be 0.4 and 0.6 ns, respectively, which are still orders of magnitude longer than the hot carrier cooling (or thermalization) time (~0.4 ps).[7] Clearly, a large amount of the converted photon energy is wasted due to thermalization, and some of the energy is also lost to carrier trapping. A variety of routes have been proposed to facilitate electron/hole extractions by taking advantage of some special materials such as fullerene,[12] graphene,[13] or core/shell metal nanoparticles,[14] but direct evidence is yet to be obtained regarding their role as a fast electron funnel rather than just an electron trapping center. Together, to improve PCE of the perovskite solar cells, faster electron injection is always desirable in competing with carrier trapping and even thermalization/cooling.

In the work reported here, we examine the effects of graphene quantum dots (GQDs),[15] inserted as an ultrathin layer between perovskite and TiO_2, on the solar cell performance. GQDs are single- or few-layer graphene but have a tiny size of only several nanometers with special quantum-confinement effects and edge effects, making them distinct from both conventional quantum dots and graphene.[16] Some unique optoelectronic properties of GQDs have already been uncovered,[17] such as hot-electron lifetimes as long as hundreds of picoseconds[18] and ultrafast hot-electron extraction (time constant <15 fs) through a GQD to TiO_2 interface.[19] In fact, GQDs were utilized as a sensitizer in a dye-sensitized solar cell,[20] but the low PCE (<0.1%) limits the further application as hot carrier chromophore, perhaps because of some not-yet-optimized materials issues. In another device configuration—organic photovoltaics—GQDs have been widely used as electron acceptors analogous to fullerenes with respect to the active layer of poly(3-hexylthiophene) (P3HT),[21,22] but they are still far inferior to fullerenes in this role, due perhaps to their lower electron affinity and less appropriate assembly morphology. To our surprise, however, the GQDs in our device configuration could serve as a superfast bridge to facilitate the electron injection from a halide perovskite into TiO_2, leading to a significantly enhanced photocurrent and PCE of the corresponding solar cells. Indeed, from the transient absorption measurements, we directly observed a faster electron extraction time (90 ps) after inserting the ultrathin GQDs layer than that (280 ps) obtained without the presence of the GQDs.

We synthesized the single-/few-layer GQDs by a facile electrochemical method reported previously.[15] The structure of GQDs is schematically illustrated in Figure 1C. In particular, the water-soluble GQDs have a modified edge structure with an average diameter of 5−10 nm (Figure S1), a broad absorption band from 200 to 400 nm (Figure S2a), and a strong photoluminescence peak at ~540 nm (Figure S2b). The perovskite solar cell devices were fabricated following the layout in Figure 1A, and the relative energy levels of the different layers are shown in Figure 1B (see Supporting Information for full

Received: January 5, 2014
Published: February 24, 2014

dx.doi.org/10.1021/ja4132246 | J. Am. Chem. Soc. 2014, 136, 3760−3763

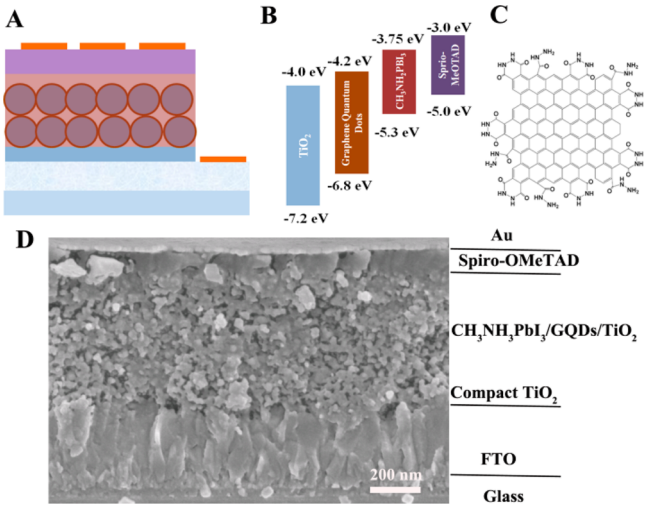

Figure 1. Schematic representation of the typical full device structure (A), where the mesoporous oxide is either loaded with GQDs or not, the energy band alignment relative to vacuum (B), and the edge-modified GQD structure determined by theoretical calculation (C).[15] (D) Cross-sectional SEM image of a complete photovoltaic device based on the $CH_3NH_3PbI_3$/GQDs/TiO_2 structure. Scale bar: 200 nm.

experimental details). The cross-sectional scanning electron microscope (SEM) image of a typical such device is shown in Figure 1D. The distribution of GQDs within the TiO_2 mesoporous film appears to be uniform according to the energy-dispersive X-ray spectroscopy (EDS) elemental mapping (Figure S3). X-ray powder diffraction patterns in Figure S4 show peaks ascribable to GQDs, TiO_2, and tetragonal $CH_3NH_3PbI_3$.[23,24]

We measured current (J)−voltage (V) characteristics of the solar cells under simulated air mass 1.5 global (AM1.5G) solar irradiation, which are designated as the perovskite $CH_3NH_3PbI_3$/GQDs/TiO_2 (or PGT for short) and the standard perovskite $CH_3NH_3PbI_3$/TiO_2 (or PT for short) solar cells, respectively. Figure S5 shows a schematic and a photograph of arrays such solid-state solar cells, each with an active area of 0.126 cm^2 (1.8 mm × 7.0 mm). Figure 2 shows J−V curves of the solar cells. The most important observation from the J−V curves is the beneficial role of the ultrathin GQDs layer between perovskite

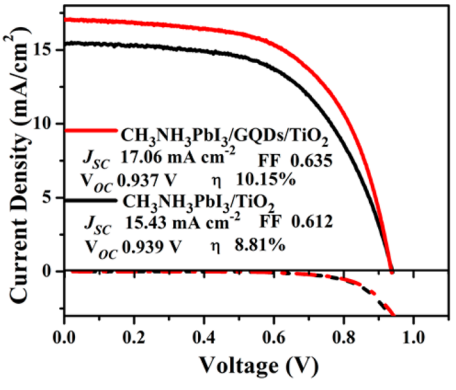

Figure 2. Current density−voltage curves for the best-performing solar cells. $CH_3NH_3PbI_3$/GQDs/TiO_2 (red line) and $CH_3NH_3PbI_3$/TiO_2 (black line) cells were measured under AM1.5G illumination at 100 mW/cm^2 (solid line). Dashed lines depict the data obtained at the dark condition.

and TiO_2: the cell with the GDQs layer achieved a power conversion efficiency (PCE) of 10.15%, whereas that without it only achieved a PCE of 8.81%. The short-circuit current density (J_{sc}) of the QD loading device of PGT has a significant increase from 15.43 to 17.06 mA/cm^2 compared with the non-GQD loading PT device, whereas the fill factor (FF) and open-circuit voltages (V_{oc}) are similar: 0.939 V and 0.612 FF for the PT device, and 0.937 V and 0.635 FF for the PGT device. The small V_{oc} change is consistent with the fact that the main role of the ultrathin GQDs layer is to facilitate the electron extraction. To investigate the effects of the loading amount of GQDs on the cell performance, we fabricated a few tens of the cells with different amounts of GQDs loaded in and measured their performance. The performance testing results of these cells are collected in the Supporting Information (see Figure S6). We found that the cells loaded with 0.5 mg/mL GQDs concentration have the best photocurrent improvement among all of the cells we have studied. Specifically, the cells with 0.5 mg/mL GQDs attained an average PCE of 9.8%, whereas those without GQDs had an average PCE of only 8.6%.

From the J−V curves of various cells described above, the improved photocurrent is almost the sole contribution to the enhanced perovskite solar cell performance achieved by the insertion of the ultrathin GQD layer. To further understand the origin of this phenomenon, a series of optical absorption and photocurrent spectroscopic studies have been carried out. The absorption spectra in Figure 3A show that there is little difference

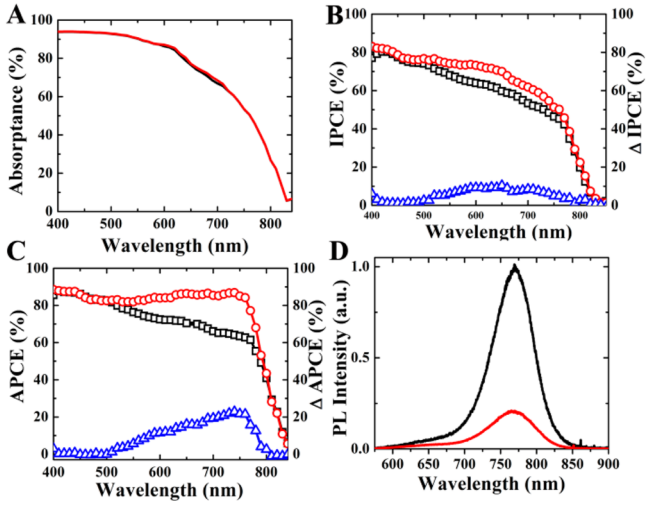

Figure 3. (A) UV/vis absorbance spectra of PGT (red line) and PT (black line). (B) IPCE spectra (the left ordinate). The right ordinate indicates the improved IPCE (ΔIPCE) due to GQDs. (C) APCE spectra derived from the IPCE and UV/vis absorbance spectra and ΔAPCE derived from the APCE change due to GQDs. Designation of the IPCE and APCE curves: PGT (red circles); PT (black squares); ΔIPCE and ΔAPCE (blue triangles). (D) PL spectra of the PGT (red line) and PT (black line) films excited at 514.5 nm (20 mW).

for the films with or without the GQDs loading. This means that the small amount of GQDs in the films had little influence on the total absorbance, which is dominated by the much more strongly absorbing and thicker perovskite layer. To confirm the enhancement of the photocurrent, we recorded incident-photon-to-current conversion efficiency (IPCE) spectra, and this result is shown in Figure 3B. The integrated photocurrent densities (Figure S7) of the IPCE spectra read 15.26 mA/cm^2 (PT) and 16.94 mA/cm^2 (PGT), respectively, which are in fairly

dx.doi.org/10.1021/ja4132246 | J. Am. Chem. Soc. 2014, 136, 3760−3763

good agreement with the corresponding measured values. Clearly, there is a significant improvement in IPCE between 500 and 750 nm when the GQD layer was inserted between the perovskite and the TiO_2 layers. By taking the difference in the IPCE spectra between the PGT and the PT devices, we obtain a ΔIPCE spectrum, which is also shown in Figure 3B. The ΔIPCE spectrum shows a broad band mostly in the visible wavelength region of 500−750 nm, peaking at ∼650 nm. After light absorbance is taken into account, the IPCE spectra can be converted to the internal quantum efficiency or absorbed-photon-to-current conversion efficiency (APCE).

The resulting APCE spectra and the corresponding ΔAPCE spectrum are shown in Figure 3C. The ΔAPCE spectrum shows that the added GQDs significantly enhanced the APCE, mainly in the long-wavelength range peaking at 750 nm. Since the GQDs monolayer absorption is expected to be small, the ΔAPCE spectrum is believed to stem primarily from absorption of the perovskite excited state influenced by the GQDs layer. Interestingly, the enhanced APCE in the longer-wavelength region corresponds to the lower-energy portion of the photogenerated electrons. Those lower-energy electrons could be more easily trapped prior to extraction when no GQD layer is present. But when the GQD layer is inserted, the electron extraction is facilitated and helps prevent the trapping events. This nicely explains why the APCE with GQDs is >85% and nearly constant in the whole visible region, whereas it keeps declining toward the long-wavelength region when the GQDs layer is not inserted.

The notion inferred above that the electron extraction is facilitated by inserting the ultrathin GQD layer is corroborated by the steady-state photoluminescence (PL) measurement. Figure 3D shows steady-state PL spectra of the PGT and PT samples, which were fabricated on sapphire substrates. Under the same experimental conditions, both PGT and PT films exhibit a PL peak at 760 nm arising from the perovskite; however, the perovskite PL quantum yield of the PGT film is largely reduced compared to that of the PT film. More specifically, the perovskite PL intensity of the PGT film is quenched by nearly 75% with respect to the PT film. Such a dramatic PL quenching is particularly interesting in solar cell development because it could be caused by the significantly enhanced charge carrier extraction arising from the added GQDs layer. Here the GQDs could play a role as an electron acceptor in much the same way as fullerenes do. Alternatively, GQDs may also act as an effective bridge that can enhance the charge injection from the perovskite to TiO_2 without actually capturing the flowing charges. Since the electron affinity of GQDs is much smaller than that of fullerenes, the latter role of GQDs may be at work, which turns out to be more significant for enhancing solar cell efficiency. In this case, the GQD layer with widely distributed π orbitals may act as an ultrathin glue and superfast electron funnel to increase the electronic coupling between the perovskite and TiO_2. Indeed, some unique electron dynamics of GQDs have already been reported,[13] such as long hot-electron lifetimes up to hundreds of picoseconds[14] and ultrafast hot-electron extraction from the GQD to TiO_2 interface within <15 fs.[15]

As a step further to understand the role of the ultrathin GQDs layer in the working solar cell device, we performed femtosecond transient absorption (fs-TA) spectroscopy[25] on the films of perovskite-coated mesoporous titanium dioxide with (PGT) and without (PT) the interlayer of GQDs. More detailed experimental procedures for the TA measurement can be found in the Supporting Information.

Figure 4A,B shows representative TA spectra of the PT and PGT films. The most obvious features associated with the

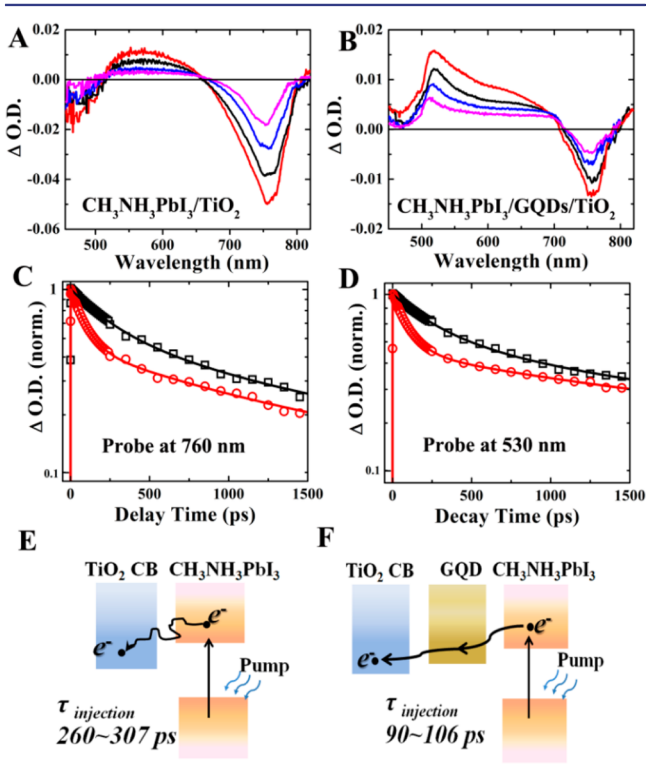

Figure 4. Transient absorption spectra of PT (A) and PGT (B) after excitation at 400 nm: red (10 ps), black (100 ps), blue (500 ps), and violet (1000 ps). Normalized kinetic traces for photobleaching (C) probed at 760 nm and photoinduced absorption (D) probed at 530 nm: PT (black square line) and PGT (red circle line). Schematic illustration of electron generation and extraction at PT (E) and PGT (F) interfaces.

perovskite $CH_3NH_3PbI_3$ are the photobleaching (PB) negative peak at around 750 nm and the photoabsorption (PA) positive peak at 500−600 nm, which are in agreement with some earlier reports.[7,8] For reference, the TA spectra of the TiO_2 and GQDs/TiO_2 films have two small but similar features with a decay time of <10 ps (see Figure S8) and thus are neglected in the discussion below. The TA spectra of the PGT and PT films at different delay times are displaced vertically to expose clearly the attendant spectral changes. The negative bleaching (PB) band observed at ∼750 nm is related to the fluorescent emission from perovskite as revealed by the steady-state PL result described above, while the positive absorption (PA) band at 500−600 nm must be due to the absorption of certain transient species. On insertion of the GQD layer (in the $CH_3NH_3PbI_3$/GQDs/TiO_2 film), the fs-TA spectral profiles show several important features distinct from those of the PT film without GQDs. First, the PGT film exhibits a remarkably stronger positive peak in the wide wavelength region from 500 to 700 nm (see Figure 4B) than the PT film (see Figure 4A), suggesting intense absorption of the perovskite-GQDs interfacial excited states (∼530 nm, slightly blue-shifted at longer delays) as well as the perovskite bulk excited states (>600 nm). Second, by comparing the PB peak at ∼760 nm between the PT and PGT films, we notice that the negative peak intensity of the latter is largely decreased. This agrees with the steady-state PL results in the sense that the presence of GQDs quenches much of the PL of perovskite due to the aforementioned GQD-facilitated electron extraction of the photogenerated electrons in the

dx.doi.org/10.1021/ja4132246 | J. Am. Chem. Soc. 2014, 136, 3760−3763

perovskite layer. For the sake of comparison below, the time evolution profiles of the PB peak at 760 nm and the PA peak at 520 nm are shown in Figure 4C,D, respectively.

To simplify the kinetic analysis of the TA data, we only consider the time evolution of the excited perovskite from 10 to 2000 ps since the decay of excited TiO_2 and GQD is relatively fast (within 10 ps, see Figure S8). The decay traces of the PA and PB features (Figure 4A,B) have been well fitted with a double exponential function (Figure 4C,D), and the relevant decay time constants are collected in Table S3. For both the PT and PGT films at the probe wavelengths of both the PB and PA features, the slower time constants are all within 2000−2300 ps, which can be ascribed to the $CH_3NH_3PbI_3$ excited-state decay time or recombination dynamics of $CH_3NH_3PbI_3$ absorber as reported previously.[7,8] However, the faster time constants of the two films are quite different. Specifically, for the PT film, the PB bleaching peak at 760 nm (Figure 4C) shows a faster decay time constant of 260 ps, while the PA absorption peak at 530 nm (Figure 4D) decays with a faster time constant of 310 ps. The two similar faster time constants are plausibly related to the electron extraction from the photoexcited $CH_3NH_3PbI_3$ to the TiO_2 conduction band. Most significantly, when the ultrathin GQDs layer is inserted between the perovskite and TiO_2, the faster decay time constant of the PB bleaching peak is dramatically reduced to 90 ps, while that of the PA absorption peak experiences a similar decrease to 106 ps. As a result, the faster decay time constants for the PA and PB peaks of the PGT film are nearly 3 times shorter than those of the PT film. Thus we have demonstrated that the electron extraction from perovskite to TiO_2 is significantly enhanced by the interlayer of GQDs, which act as an ultrathin glue for enhancing the electronic coupling and as a superfast electron funnel for efficiently mediating the electron transfer from the absorber to acceptor. Although ultrafast hot electron extraction from GQDs to TiO_2 has been reported previously, this is the first time such GQD-mediated fast electron extraction from perovskite to TiO_2 was directly observed. Future theoretical studies should help to clarify the mechanism involved.

In conclusion, we have designed a high-efficiency (>10%) perovskite solar cell by inserting an ultrathin layer of GQDs between the perovskite and the mesoporous titanium dioxide, and this efficiency is significantly higher than the 8.81% efficiency without GQDs. The efficiency enhancement is shown to be mostly ascribable to the boosting of the photocurrent. The IPCE and APCE spectra show a significantly enhanced absorbed photon-to-current conversion in the visible to the near-infrared regions resulting from the GQDs loading. By virtue of the ultrafast transient absorption spectroscopy measurements, we found a considerably faster electron extraction time at 90−106 ps in the PGT film than in the PT film (260−307 ps), which could effectively compete with carrier trapping and thus provide a reasonable explanation to the GQDs-induced cell performance enhancement. This finding highlights the beneficial role of GQDs in facilitating the electron transfer from the perovskie absorber to the current collector, other than its conventional role as electron acceptor in OPV cells. Further work on GQDs accelerated electron injection may allow hot carrier extraction before cooling down to the band edges, opening up new pathways for future developments of new generation solar cells.

■ ASSOCIATED CONTENT

Supporting Information

Experimental details and additional tables and figures. This material is available free of charge via the Internet at http://pubs.acs.org.

■ AUTHOR INFORMATION

Corresponding Authors

lzfan@bnu.edu.cn

chsyang@ust.hk

Notes

The authors declare no competing financial interest.

■ ACKNOWLEDGMENTS

This work was supported by the HK-RGC General Research Funds (HKUST 606511 and 605710) and the Major ResearchPlan of NSFC (21233003). Partial support from AoE/P-03/08 and SEG HKU/07 is also acknowledged.

■ REFERENCES

(1) Chu, S.; Majumdar, A. *Nature* **2012**, *488*, 294.

(2) Kojima, A.; Teshima, K.; Shirai, Y.; Miyasaka, T. *J. Am. Chem. Soc.* **2009**, *131*, 6050.

(3) Etgar, L.; Gao, P.; Xue, Z.; Peng, Q.; Chandiran, A. K.; Liu, B.; Nazeeruddin, M. K.; Graetzel, M. *J. Am. Chem. Soc.* **2012**, *134*, 17396.

(4) Chen, Q.; Zhou, H.; Ziruo, H.; Luo, S.; Duan, H.; Wang, H.; Liu, Y.; Li, G.; Yang, Y. *J. Am. Chem. Soc.* **2014**, *136*, 622.

(5) Burschka, J.; Pellet, N.; Moon, S. J.; Humphry-Baker, R.; Gao, P.; Nazeeruddin, M. K.; Gratzel, M. *Nature* **2013**, *499*, 316.

(6) Liu, M.; Johnston, M. B.; Snaith, H. J. *Nature* **2013**, *501*, 395.

(7) Xing, G. C.; Mathews, N.; Sun, S. Y.; Lim, S. S.; Lam, Y. M.; Gratzel, M.; Mhaisalkar, S.; Sum, T. C. *Science* **2013**, *342*, 344.

(8) Stranks, S.; Eperon, G.; Grancini, G.; Menelaou, C.; Alcocer, M. P.; Leijtens, T.; Herz, L.; Petrozza, A.; Snaith, H. *Science* **2013**, *342*, 341.

(9) Janssen, R. A. J.; Nelson, J. *Adv. Mater.* **2013**, *25*, 1847.

(10) McGehee, M. D. *Nature* **2013**, *501*, 323.

(11) Park, N. G. *J. Phys. Chem. Lett.* **2013**, *4*, 2423.

(12) Abrusci, A.; Stranks, S. D.; Docampo, P.; Yip, H. L.; Jen, A. K. Y.; Snaith, H. *Nano Lett.* **2013**, *13*, 3124.

(13) Wang, J.; Ball, J.; Barea, E.; Abate, A.; Alexander-Webber, J.; Huang, J.; Saliba, M.; Mora-Sero, I.; Bisquert, J.; Snaith, H.; Nicolas, R. *Nano Lett.* **2014**, *14*, 724.

(14) Zhang, W.; Saliba, M.; Stranks, S. D.; Sun, Y.; Shi, X.; Wiesner, U.; Snaith, H. *Nano Lett.* **2013**, *13*, 4505.

(15) Zhang, M.; Bai, L.; Shang, W.; Xie, W.; Ma, H.; Fu, Y.; Fang, D.; Sun, H.; Fan, L.; Han, M.; Liu, C.; Yang, S. H. *J. Mater. Chem.* **2012**, *22*, 7461.

(16) Yan, X.; Li, B. S.; Li, L. S. *Acc. Chem. Res.* **2013**, *46*, 2254.

(17) Zhang, Z.; Zhang, J.; Chen, N.; Qu, L. *Energy Environ. Sci.* **2012**, *5*, 8869.

(18) Mueller, M. L.; Yan, X.; Dragnea, B.; Li, L. *Nano Lett.* **2011**, *11*, 56.

(19) Williams, K.; Nelson, C.; Yan, X.; Li, L.; Zhu, X. *ACS Nano* **2013**, *7*, 1388.

(20) Yan, X.; Cui, X.; Li, B.; Li, L. *Nano Lett.* **2010**, *10*, 1869.

(21) Li, Y.; Hu, Y.; Zhao, Y.; Shi, G.; Deng, L.; Hou, Y.; Qu, L. *Adv. Mater.* **2011**, *23*, 776.

(22) Gupta, V.; Chaudhary, N.; Srivastava, R.; Sharma, G. D.; Bhardwaj, R.; Chand, S. *J. Am. Chem. Soc.* **2011**, *133*, 9960.

(23) Liang, K. N.; Mitzi, D. B.; Prikas, M. *Chem. Mater.* **1998**, *10*, 403.

(24) Qiu, J. H.; Qiu, Y. C.; Yan, K. Y.; Zhong, M.; Mu, C.; Yan, H.; Yang, S. H. *Nanoscale* **2013**, *5*, 3245.

(25) Ma, J.; Su, T.; Li, M.-D.; Du, W.; Huang, J.; Guan, X.; Phillips, D. L. *J. Am. Chem. Soc.* **2012**, *134*, 14858.